Article

Zonal human hepatocytes are differentially permissive to *Plasmodium falciparum* malaria parasites

Annie S P Yang[1],* (iD), Youri M van Waardenburg[1], Marga van deVegte-Bolmer[1],
Geert-Jan A van Gemert[1], Wouter Graumans[1], Johannes H W de Wilt[2] & Robert W Sauerwein[1],**,† (iD)

Abstract

Plasmodium falciparum **(*Pf*) is a major cause of human malaria and is transmitted by infected *Anopheles* mosquitoes. The initial asymptomatic infection is characterized by parasite invasion of hepatocytes, followed by massive replication generating schizonts with blood-infective merozoites. Hepatocytes can be categorized by their zonal location and metabolic functions within a liver lobule. To understand specific host conditions that affect infectivity, we studied *Pf* parasite liver stage development in relation to the metabolic heterogeneity of fresh human hepatocytes. We found selective preference of different *Pf* strains for a minority of hepatocytes, which are characterized by the particular presence of glutamine synthetase (hGS). Schizont growth is significantly enhanced by hGS uptake early in development, showcasing a novel import system. In conclusion, *Pf* development is strongly determined by the differential metabolic status in hepatocyte subtypes. These findings underscore the importance of detailed understanding of hepatocyte host-*Pf* interactions and may delineate novel pathways for intervention strategies.**

Introduction

Malaria is a devastating mosquito-borne disease responsible for approximately 220 million clinical cases and 430,000 deaths annually (WHO, 2018). It is caused by the parasites of the *Plasmodium* genus, of which *P. falciparum* (*Pf*) is responsible for most of the disease burden. The infection begins with deposition of sporozoites in the skin by blood-feeding infected mosquitoes. Subsequently, low numbers of deposited sporozoites invade, differentiate, and massively multiply (as schizont forms) inside hepatocytes followed by release of blood-infective merozoites via merosomes into the circulation in rodent malaria models (Sturm *et al*, 2006). Cycles of asexual parasite multiplication in circulating red blood cells are responsible for malaria morbidity and mortality (Mo & McGugan, 2018).

Interaction between host hepatocytes and parasites, especially intracellular host factors that influence parasite development, is poorly understood. Studies of *Pf* parasites and host cells, primarily studied with the NF54 strain, are hampered by low parasite infection rates of *in vitro* cultured hepatocytes (Roth *et al*, 2018). Large "omics-based" approaches have been previously applied in rodent malaria models (Tarun *et al*, 2008; Shears *et al*, 2019), but translational relevance to *Pf* parasites suffers from important biological differences between the two species, i.e. the much shorter liver stage of 48 h (rodent models) as compared to 7 days (*Pf*).

The liver is a complex organ, composed of functional lobules where hepatocytes express distinct metabolic functions related to their zonal location (Z) (Jungermann & Kietzmann, 1996). Hepatocytes of a particular zone do express specific sets of genes reflective of their differential tasks related to glucose metabolism (Halpern *et al*, 2017; Aizarani *et al*, 2019; Ben-Moshe *et al*, 2019). As such, periportal Z1 is involved in gluconeogenesis during homeostasis while Z3 generates energy through glycolysis (Gumucio & Miller, 1981; Jungermann, 1983). Glucokinase (GK) is an important cytoplasmic enzyme of glycolysis, catalysing the first step of converting glucose to glucose-6-phosphate (Katz *et al*, 1977; Fischer *et al*, 1982). In a gluconeogenic state, i.e. Z1, GK is sequestered away from the cytoplasm, being inhibited by its regulatory protein (GKRP) and adopts a nuclear localization (Toyoda *et al*, 1995; Jetton *et al*, 2001). Contrastingly in Z3, GK translocates from the nucleus to the cytoplasm to participate in glycolysis. Additionally, Z3 hepatocytes are characterized by the exclusive presence of glutamine synthetase (GS), the only so-called stable marker of liver zonation, i.e. not

---

1   Radboudumc Center for Infectious Diseases, Department of Medical Microbiology, Radboud University Medical Center, Nijmegen, The Netherlands
2   Department of surgery, Radboud University Medical Center, Nijmegen, The Netherlands
    *Corresponding author. Tel: +31 (0) 24 361 3663; E-mail: annie.yang@radboudumc.nl
    **Corresponding author. Tel: +31 (0) 24 366 6478; E-mail: robert.sauerwein@radboudumc.nl
    †Present address: TropIQ Health Sciences, Nijmegen, The Netherlands

affected by the glucose availability of the host (Jungermann & Kietzmann, 1996). Z2 are located in between Z1 and 3 with apparent limited ability to perform both gluconeogenesis and glycolysis.

The unique intracellular environments present in hepatocytes of different zones may influence the developmental kinetics of obligate intracellular microbes, including *Pf* parasites. *Pf* liver stages represent an attractive target for vaccine and/or drug development but progress is hindered by limited knowledge of the molecular and cellular events that occur during this stage (Mo & McGugan, 2018). While host-*Pf* interactions have been mostly focused on hepatocyte membrane receptors allowing for *Pf* entry (Silvie *et al*, 2003; Rodrigues *et al*, 2008; Yalaoui *et al*, 2008), the intracellular milieu may have major impact on parasite development. Here, we examined whether freshly isolated hepatocytes characterized by hGK and/or hGS expression express differential permissiveness to a panel of clinical *Pf* isolates and explored possible mechanisms involved.

Results

Quantification of zonal hepatocytes from freshly isolated primary human hepatocytes (fPHH)

Using specific antibodies against glucokinase (hGK) and glutamine synthetase (hGS), we quantified the proportion of hepatocyte subpopulations fPHH (Fig EV1A and B for anti-hGS characterization). Z1 was defined by a stronger nuclear hGK signal compared to Z2 with concomitant lack of hGS signals; Z3 was defined by strong cytoplasmic hGS expression combined with an absence of nuclear hGK (Fig 1A–C). The fPHH monolayers (Fig 1D) from four different human donors were characterized: The vast majority of cells (90%) were Z2 hepatocytes (Z2/hGK+/GS−) with the remaining 10% being made up by Z1 (3%; Z1/hGK++/GS−) and Z3 (7%; Z3/hGK−/GS+).
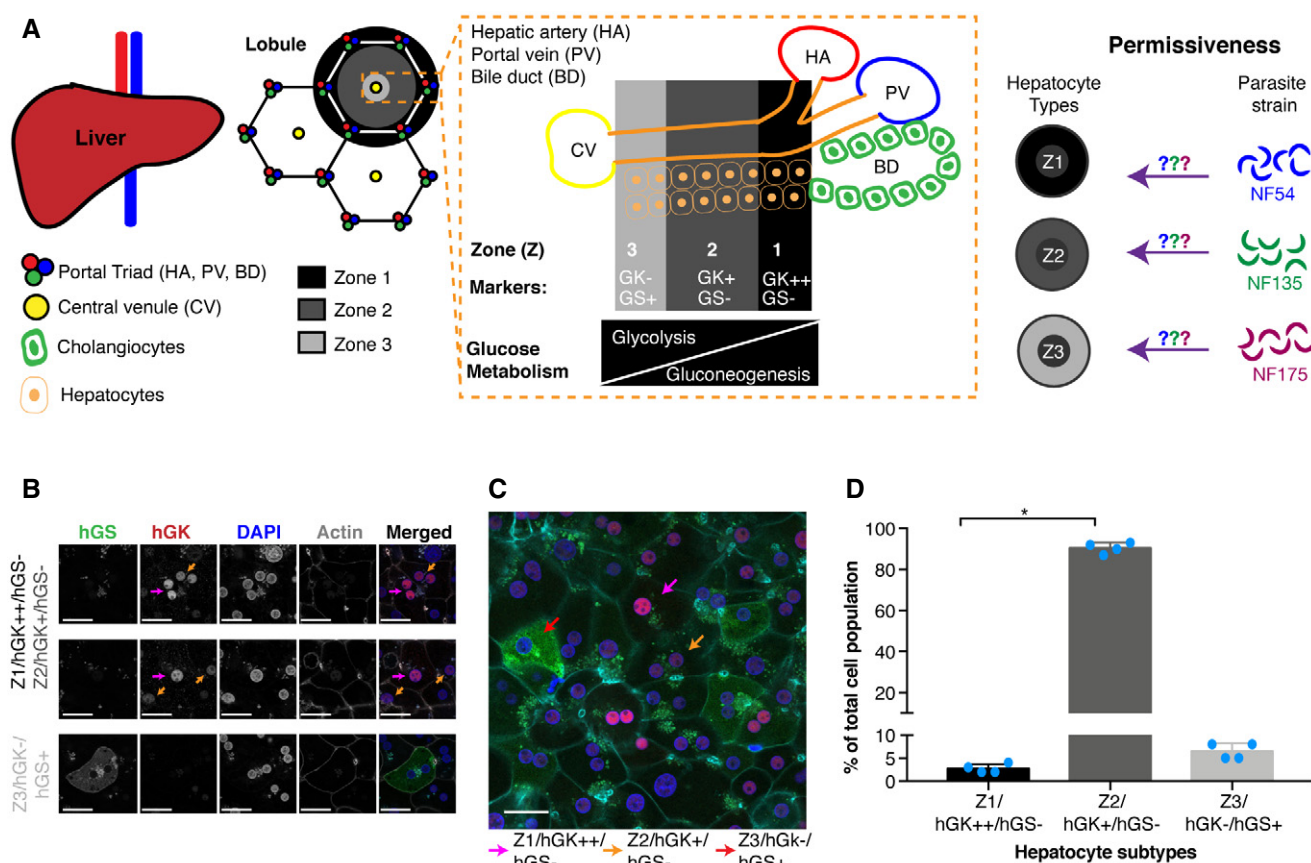

Figure 1. Characterization of zonal hepatocytes from freshly isolated human hepatocytes (fPHH).

A   Schematic of liver architecture and underlying objective of the study.
B   Confocal immunofluorescence image of fPHH at 5 days post-plating stained with hGK (red), hGS (green), DAPI (blue) and phalloidin (grey). Objective 63×; zoom 2×; scale bar 25 μm.
C   Confocal immunofluorescence image of a fPHH monolayer at 5 days post-plating, stained with hGK (red), hGS (green), DAPI (blue) and phalloidin (cyan). Arrow point towards a typical hepatocyte subpopulation shown by different colours. Objective 40×; scale bar 25 μm.
D   Percentage of zone 1–3 uninfected hepatocytes day 5 post-plating (± s.d.) of 4 different donors (blue dots). For each donor, > 500 cells were characterized for the final percentages. Kruskal–Wallis test ($P = 0.0002$) followed by Dunn's multiple comparisons test where Z1/hGK++/hGS− vs. Z2/hGK+/hGS− has a P value of 0.0140 (the other comparisons of Z1/hGK++/hGS− vs. Z3/hGK−/hGS+ and Z2/hGK+/hGS− vs. Z3/hGK−/hGS+ were non-significant).

Source data are available online for this figure.

Permissiveness of hepatocyte subsets for Pf strains

Established *Pf* strains differed genotypically at a selection of gene loci (Fig 2A and B) but did express typical markers used to characterize *Pf* liver stages (Fig 2C). Both NF135 (McCall *et al*, 2017; Langenberg *et al*, 2018) and NF175 (Graumans *et al*, 2019) showed approximately 4-fold higher numbers of infected fPHH at multiple time points post-invasion (p.i.) (Fig 3A) and were significantly

larger in size (Fig 3B) compared to NF54 using high content fluorescence microscopy (see Materials and Methods section: Data analysis using FIJI, Infection rate).

Next, we determined the percentage of *Pf* strains located in different hepatocyte subpopulations on day 3 p.i. (Fig 3C). As the hGS antibody interfered with antibody used to visualize parasites (being of the same animal species), only the hGK antibody (red) was used to characterize the hepatocyte subpopulations. Phalloidin was used
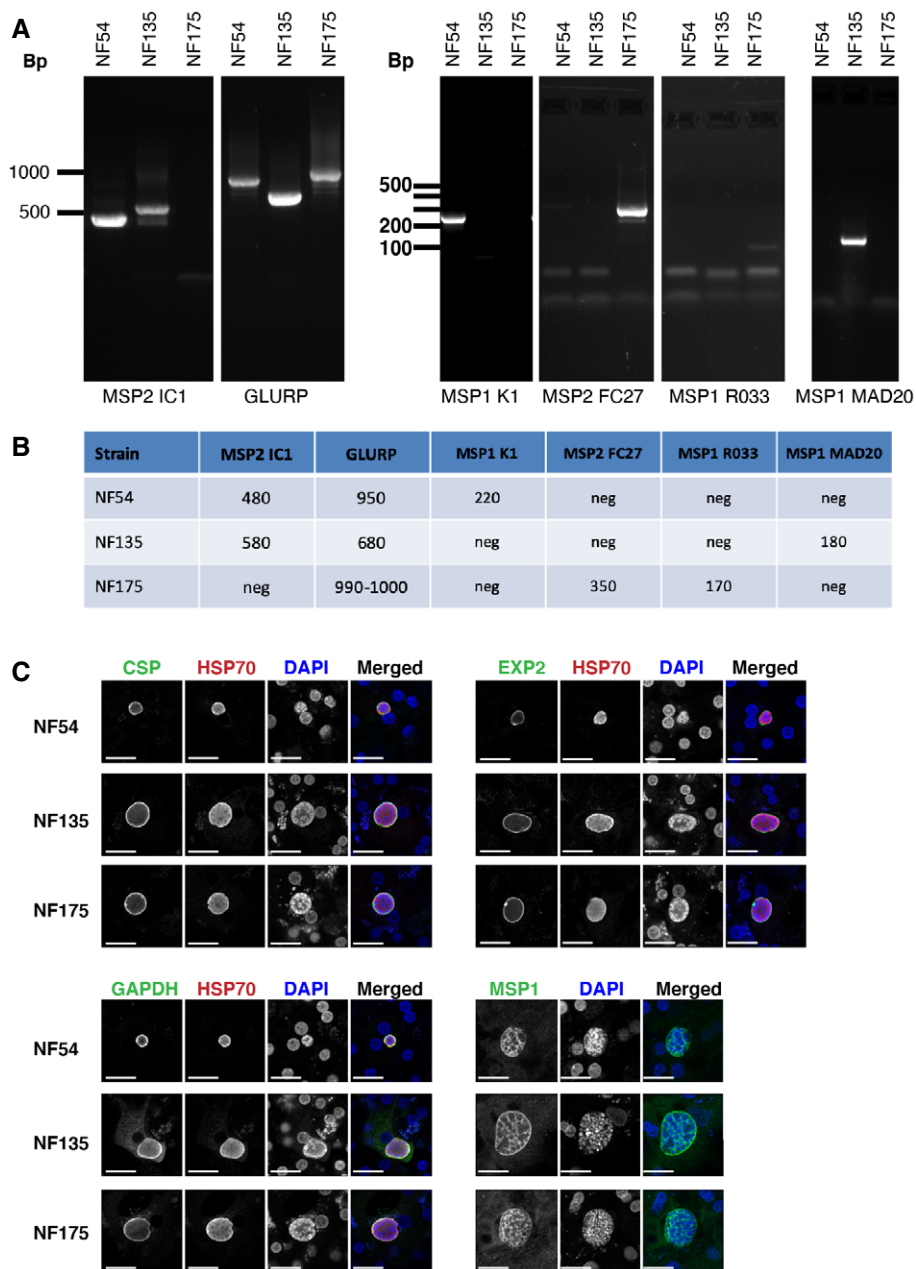

Strain	MSP2 IC1	GLURP	MSP1 K1	MSP2 FC27	MSP1 R033	MSP1 MAD20
NF54	480	950	220	neg	neg	neg
NF135	580	680	neg	neg	neg	180
NF175	neg	990-1000	neg	350	170	neg

Figure 2. Characterization of NF54, NF135 and NF175.

A   Molecular characterization by PCR using established markers: MSP2 IC1, GLURP, MSP1 K1, MSP2 FC27, MSP1 R033, and MSP1 MAD20.
B   The band sizes of the markers in A for the three parasite strains.
C   Expression of typical liver stage protein markers: Circumsporozoite protein (CSP) top left; Exported Protein 2 (EXP2) top right; Glyceraldehyde 3-phosphate dehydrogenase (GAPDH) bottom left; and Merozoite surface protein 1 (MSP1) bottom right. Scale bar is 25 μm.

to stain actin, i.e. cytoskeleton of hepatocytes so the parasite schizont can be attributed to the correct host nuclei for characterization of the type of zone. The percentages of schizonts in Z1/hGK++/hGS− were similar for all three strains. Most schizonts were found in Z2/hGK+/hGS− cells, representing the majority of cells (Fig 3D). NF135 and NF175 showed relatively higher preference for Z3/hGK−/hGS+ with up to 35% infection of these cells (Fig 3E). NF54 showed slight preference for both Z3/hGK−/hGS+ (3%) and Z1/hGK++/hGS− (4%) hepatocytes, but overall infection rates and schizont size across the zones were low (Fig 3E and F). The observed distribution of infection may be the reflection of limited availability of preferred fPHHs. Therefore, graded numbers of sporozoites were added to fPHHs and infection rates were determined on day 5 p.i. Infection rates peaked at sporozoites: hepatocytes ratio of 4:1 for all three strains with higher ratios resulting in a decrease in the number of infected cells, most likely due to deterioration of the monolayer (Fig 3G and H).

Differential usage of human glutamine synthetase by Pf strains

As the majority of the parasite strains appeared to show a strong preference for Z3/hGK−/hGS+ cells, we further investigated a possible role of hGS in parasite development because of its exclusive presence in this subset. In uninfected hepatocytes, hGS molecules were uniformly distributed in the cytoplasm, but in infected cells, they clustered around the periphery and centre of developing NF135 and NF175 schizonts (Fig 4A and B). This condense and centralized accumulation of intra-parasitic hGS further transformed into network-like structures between days 5–7. Interestingly, such distribution was not found for NF54 schizonts (Fig 4C).
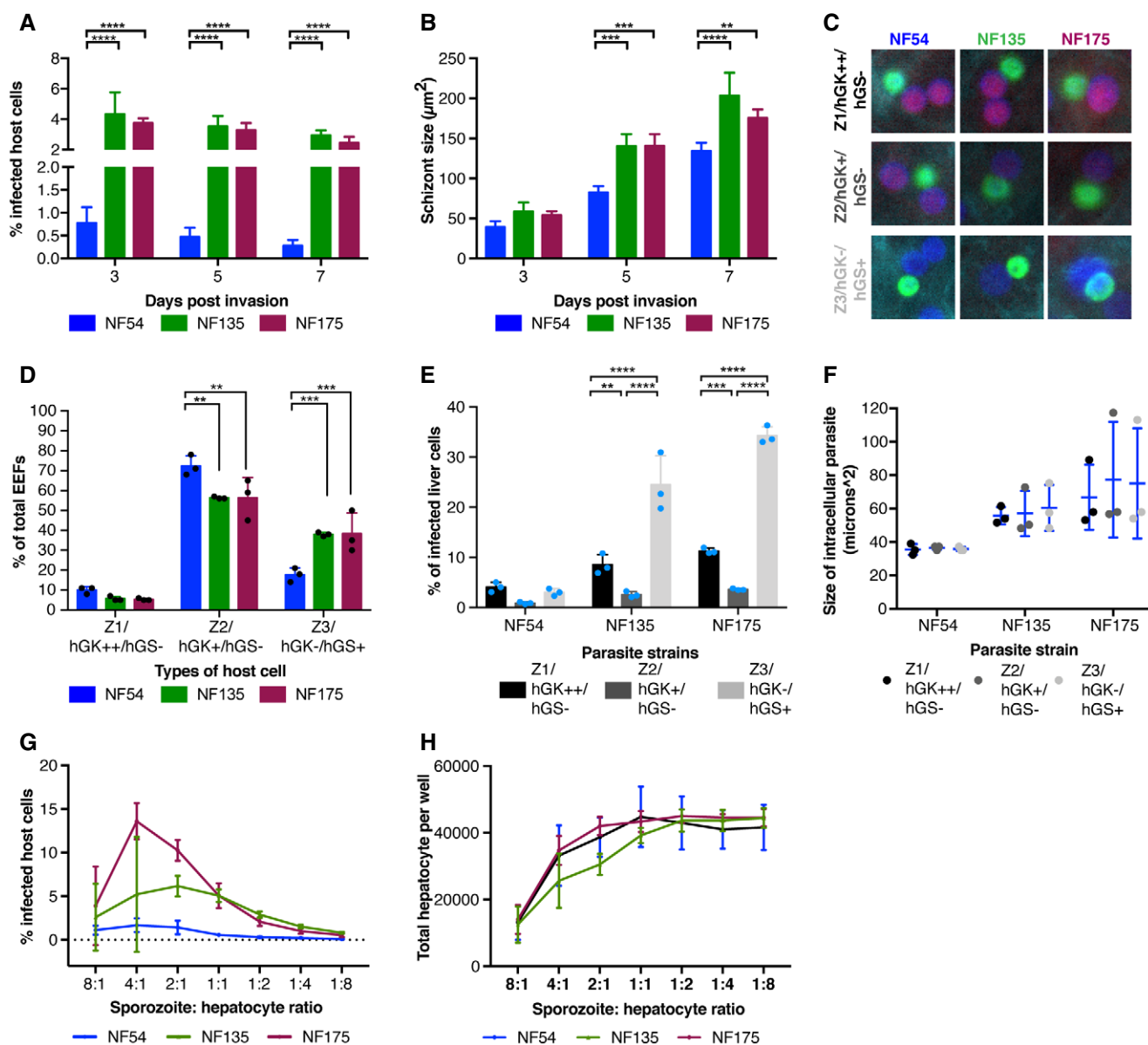

Figure 3.

Figure 3. *Plasmodium falciparum* development in fPHH and their preference for different hepatocyte subpopulations.

A, B Percentage of hepatocytes with schizonts (±s.d.) and (B) median size of schizonts (±s.d.) for NF54 (blue), NF135 (green), and NF175 (purple) on days 3, 5 and 7 p.i. with sporozoites to hepatocyte ratio of 1:1. Three biological replicates were performed with two technical replicates in each. The mean number of schizonts for the replicates per biological replicates per strain were used for the two-way RM ANOVA test, followed by a Tukey's multiple comparison test. (Mean schizonts per well ± SDS. NF54 D3 302.5 ± 55.477; D5 187.8 ± 61.087; D7 115 ± 29.360. NF135 D3 1,555.5 ± 340.4; D5 1,284.7 ± 355.4; D7 1,138 ± 251.6. NF175 D3 1,738 ± 172.679; 1,571.8 ± 84.101; 1,212.2 ± 206.7). At least 100 schizont sizes were measured for each of three biological replicates and the median is plotted above as the size distribution was not of normal distribution via the D'Agostino and Pearson normality test. The median size per strain for three biological replicates was used in a RM ANOVA test followed by a Tukey's multiple comparison test.

C Representative immunofluorescence images showing the different subpopulation of infected fPHH: hGK (red), DAPI (blue) and phalloidin (cyan). Parasites are stained with PfGAPDH (green). Images taken on the Leica High Content at 20× magnification and then cropped in Adobe Photoshop.

D Percentage of schizonts (from total number of schizonts in a well ±s.d.) located in the different hepatocyte subpopulations by NF54, NF135, NF175 on day 3 p.i. Each dot represents a biological replicate. For each parasite line, at least 100 schizonts were characterized from 2× 96 wells for the final percentage. The values from three biological replicates were used in a RM ANOVA test followed by a Tukey's multiple comparison test. Percentage of schizonts in Z1/hGK++/hGS− hepatocytes is not different between the three parasite strains. Percentage of schizonts in Z2/hGK+/hGS− for NF54 is significantly different from NF135 ($P = 0.0015$) and NF175 ($P = 0.0015$). Percentage of schizonts in Z3/hGK−/hGS+ hepatocytes for NF54 is significantly different from NF135 ($P = 0.0002$) and NF175 ($P = 0.0002$).

E Percentage (±s.d.) of Z1/hGK++/hGS− (black), Z2/hGK+/hGS− (dark grey) and Z3/hGK−/hGS+ (light grey) hepatocytes that are infected with different *Pf* strains on day 3 p.i. This is calculated by dividing the number of schizonts by the actual number of hepatocytes in each zonal subpopulation. Each dot represents a different liver donor (same donors as used in Fig 2D). The values from three biological replicates were used in a RM ANOVA test followed by a Tukey's multiple comparison test. The percentage of Z1/hGK++/hGS− and Z3/hGK−/hGS+ hepatocytes infected with parasites were different for NF135 ($P = 0.0099$ and < 0.0001, respectively) and NF175 ($P = 0.0013$ and < 0.0001, respectively) compared to NF54. The percentage of Z2/hGK+/hGS− hepatocytes infected with parasites were not significantly different between the strains. For NF135 (Z1/hGK++/hGS− vs. Z2/hGK+/hGS− = 0.0099; Z1/hGK++/hGS− vs. Z3/hGK−/hGS+ and Z2/hGK+/hGS− vs. Z3/hGK−/hGS+ < 0.0001) and NF175 (Z1/hGK++/hGS− vs. Z2/hGK+/hGS− = 0.0013; Z1/hGK++/hGS− vs. Z3/hGK−/hGS+ and Z2/hGK+/hGS− vs. Z3/hGK−/hGS+ < 0.0001), there are significant differences between the percentage of infected hepatocytes within the different zones. There is no difference in the percentage of infected hepatocytes in the different zones for NF54.

F Size of schizonts in Z1/hGK++/hGS−, Z2/hGK+/hGS− and Z3/hGK−/hGS+ hepatocytes on day 3 post-invasion for the different *Pf* strains. For each parasite line, at least 100 schizonts were measured from each biological replicate. The median values ±s.d. (as the sizes within the population is not normally distributed) from three biological replicates were used in a RM ANOVA test followed by a Tukey's multiple comparison test.

G Percentage (±s.d.) of fPHH with NF54, NF135, and NF175 schizonts on day 5 p.i., under different parasite to hepatocyte ratios (starting from 8 sporozoites to 1 hepatocyte to 1 sporozoites to 8 hepatocytes). Two biological replicates were performed with two technical replicates in each.

H Total number of hepatocytes per well (±s.d.) for NF54, NF135 and NF175 on day 5 p.i., under different parasite to hepatocyte ratios (starting from 8 sporozoites to 1 hepatocyte to 1 sporozoites to 8 hepatocytes). Two biological replicates were performed with two technical replicates in each.

Data information: *$P < 0.05$; **$P < 0.005$; ***$P < 0.001$; ****$P < 0.0001$.
Source data are available online for this figure.

Developing schizonts were categorized by strain for the presence and distinctive staining pattern of hGS (Fig 4D, Appendix Fig S1A–I). hGS + NF135 and NF175 schizonts were significantly larger than their hGS- counterparts on day 5 and 7 p.i. This could not be studied for NF54 given only very few GS+ schizonts were found from day 5 p.i. onwards. Subjectively, the relationship between intra-schizont hGS levels and size was examined for NF135 and NF175 (Figs 5A and B, and EV2A–I, and Appendix FigS2A–D; see Material and Methods: Quantifying intracellular hGS by immunofluorescence). Linear regression lines for each strain showed steeper slopes on day 3 than 5 (Fig 5C). Similarly, hGS levels strongly correlated with schizont size (Fig 5D and E) in particular on day 3.

Effect of GS inhibitors on intra-hepatic parasite development

To confirm the functionality of intra-schizont hGS and its involvement in size regulation, fPHH monolayers infected with either NF135 (hGS benefit) or NF54 (no hGS benefit) were incubated with a panel hGS inhibitors with different modes of action including Glufosinate-ammonium (GA—also known as phosphinothricin) (Gill & Eisenberg, 2001; Seabra *et al*, 2012), L-methionine sulfoximine (LMS), and 3-aminoimidazole [1,2-a] pyridine (AIP) (Ronzio *et al*, 1969; Rowe *et al*, 1969). LMS and GA compete with the substrate glutamate for the active site; the more recently discovered inhibitor AIP (Odell *et al*, 2009; Mowbray *et al*, 2014) binds to the ATP binding site of the enzyme. AIP significantly reduced the size of developing NF135 schizonts, whereas both GA and LMS were inactive (Fig 6A; Appendix Figs S3A–I and S4A–I). Addition of the

inhibitors did not affect number of intracellular parasites as expected (Fig 6C) nor seemed to affect host cell viability (Fig 6D). NF54 schizonts were not affected. Importantly, the AIP-induced size reductions were exclusively observed in hGS-positive schizonts, strengthening the functionality of hGS for parasite growth (Fig 6B). Both GA and LMS showed no activity (Appendix Figs S3A–I and S4A–I), which may be due to active metabolization in Z3 hepatocytes (Tachikawa *et al*, 2018).

Finally, we examined the timing of functional hGS on schizont size. AIP was added for 48 h to NF135 infected fPHH culture before and after parasite invasion p.i. There was a steady decrease of intracellular schizont size from day −1 onwards with maximum reduction on day 1 p.i. (Fig 6E). Similarly, size differences between hGS-positive and hGS-negative schizonts gradually decreased from day −1 onwards (Fig 6E). The relative larger effect of AIP on day 1 p.i. suggests early modulation of schizonts size by hGS; it fits well with the immunofluorescence data regarding localization (Fig 4A) and the strong correlation of hGS-positive NF135 and NF175 parasites on day 3 rather than 5 (Fig 5A–E).

Discussion

In this study, we show that intracellular *Pf* development in the liver is strongly guided by the glucose metabolic status of particular hepatocyte subpopulations. The glycolytic mode and the exclusive presence of hGS in Z3 hepatocytes are beneficial for intra-hepatic stages of particular *Pf* strains as reflected by the larger schizont sizes
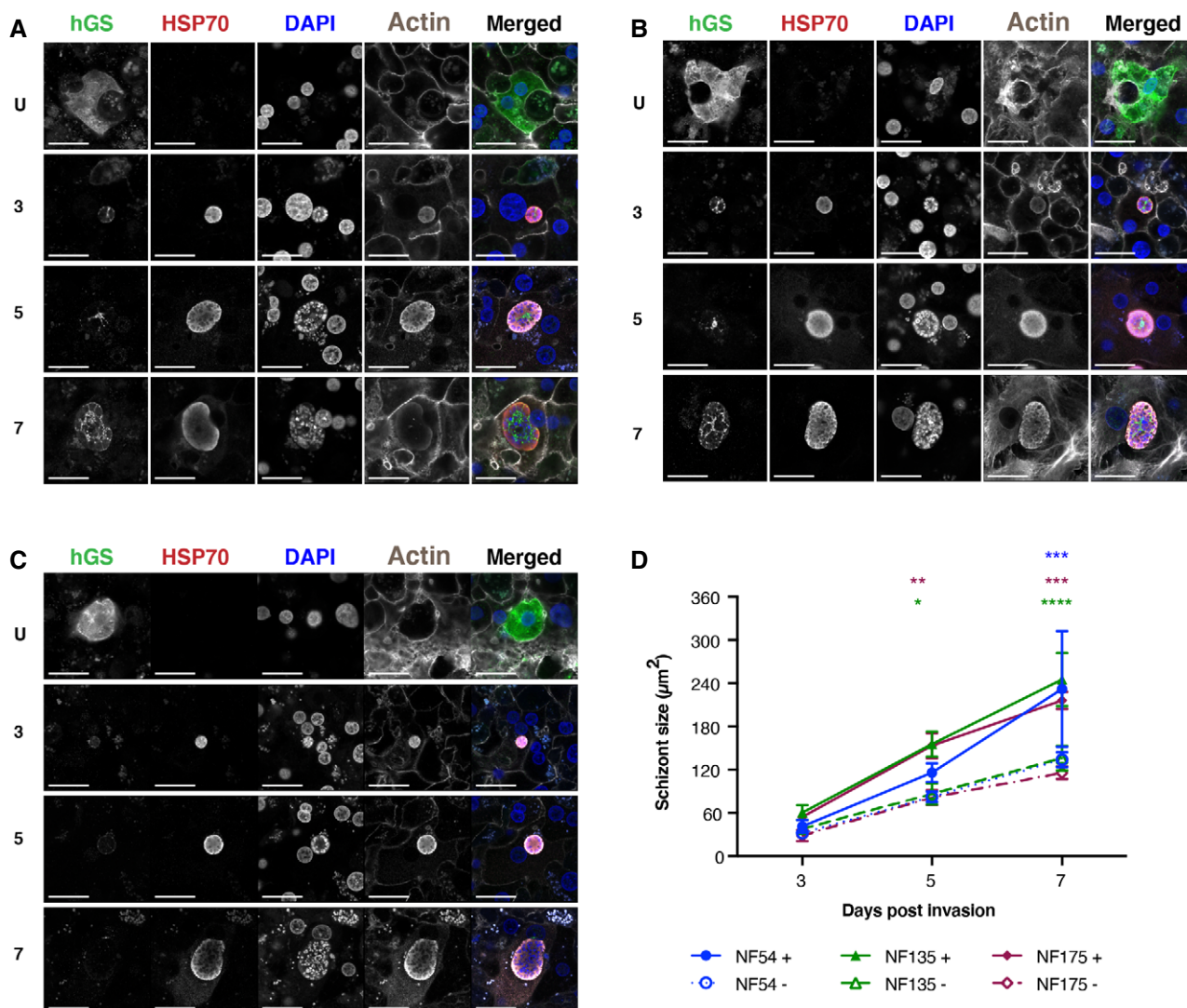
Figure 4. Distribution of human glutamine synthetase (hGS) in different *Pf* strains.

A–C   hGS interaction with NF135 (A), NF175 (B) and NF54 (C) schizonts on days 3 (top), 5 (middle) and 7 (bottom) p.i. hGS (green), *Pf*HSP70 (red), DAPI (blue) and phalloidin (grey). The U panel is composed an uninfected zone 3 hepatocyte on day 3 p.i. Scale bar is 25 μm.

D   Median sizes (±s.d.) of NF135 (green), NF175 (purple) and NF54 (blue) schizonts divided based on the presence (solid line) or absence (dashed line) of hGS staining pattern based on high content fluorescence microscopy from three different liver donors where each donor has at least 100 schizonts were measured for each of three biological replicates. A two-way RM ANOVA was performed on the median followed by a Tukey's multiple comparisons test. The significant differences between hGS+ and hGS− population within a strain is showed with asterisks (*$P < 0.05$; **$P < 0.005$; ***$P < 0.001$; ****$P < 0.0001$). See Appendix Fig S1 for the raw measurements.

Source data are available online for this figure.

(NF135 and NF175). The importance of host glucose metabolic status is in agreement with previous findings where *Plasmodium* parasites modulate the host energy sensor, AMP-activated protein kinase (AMPK) to presumably modulate glucose metabolism during liver stage development (Ruivo *et al*, 2016). Furthermore, the antidiabetic drug metformin effectively reduces the size of *Pf* liver schizonts (Vera *et al*, 2019). Metformin promotes binding of hGK to GKRP, resulting in a nuclear localization reminiscence of a Z1/2 phenotype (Guigas *et al*, 2006), shown to result in smaller schizonts in this study.

The observed differences in schizont size of NF135 and NF175 vs. NF54 can be explained by the larger number of hGS+ schizonts of the former strains. hGS-negative schizonts of all three strains are comparable in size at all time points p.i. NF54 differs in infectivity, schizont size, host cell preference, and hGS utilization from NF135 and NF175. Despite being able to reach Z3 hepatocytes on day 3 pi, NF54 seems unable to make use of host hGS. The lack of hGS-positive NF54 on day 5 and 7 is suggestive of poor survival in the Z3 environment. It remains elusive why NF54 while present in Z3 cells apparently lacks the capacity to
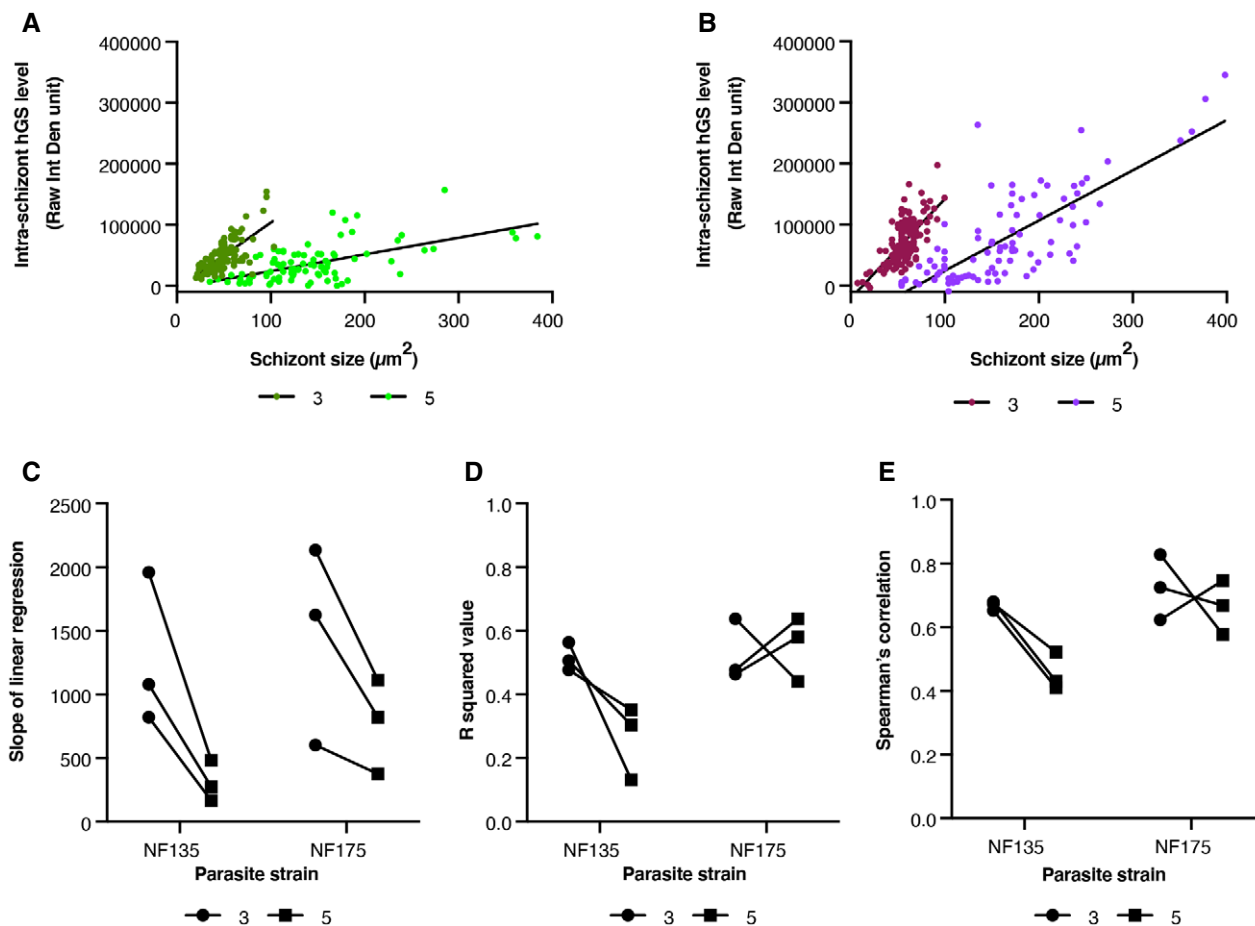
Figure 5. **Correlation between intra-parasitic hGS levels and schizont size on day 3 and 5 post-invasion.**

A, B   The total hGS signal within intracellular NF135 and (B) NF175 schizonts on day 3 and 5. Each graph represents a biological replicate where each dot represents an individual schizont.

C   The slope of the linear regression of the (A) and (B) of NF135 and NF175 on day 3 (circle) and day 5 (square) p.i.

D   The R squared value of the predicted linear relationship of hGS levels vs. schizont size on day 3 and day 5 p.i.

E   The Spearman's correlation coefficient between hGS levels and schizont size of NF135 and NF175 on day 3 and day 5 p.i.

Data information: For C–E: Each dot represents one biological replicate. See Appendix Fig S2A–D for raw data.

mobilize hGS for its own benefit. Furthermore, NF54 parasite development in all hepatocyte subtypes are inferior than NF135 and NF175. Together, it suggests that the observed differences in intracellular parasite numbers between NF54 and NF135/NF175 are due to an inability to make use of hGS that boost schizont development.

Glutamine, as end product of hGS, has been shown to be critical for rapidly proliferating cells; its nitrogen is needed for purines (adenosine and guanine) involved in DNA replication and as building block for newly synthesized proteins and lipids (Curi *et al*, 2005; Cory & Cory, 2006). In this study, this results in the generation of larger schizonts presumably due to more robust DNA, protein, and lipid production. The uptake of hGS by certain parasite strains is indicative of an import pathway which may also be involved in the direct transport of other host factors into the parasite. Understanding the timing and mechanism of this pathway may prove to be useful as a direct delivery platform of anti-malarials, bypassing the

parasitophorous and parasite membranes. This may be particularly important as *Pf* liver stages represent an attractive target for clinical interventions.

The parasite-induced redistribution of intracellular hGS, may also have direct consequences for hepatocyte survival. Mammalian host cells are equipped with intrinsic detection systems that prevent existence and/or replication of pathogens. High intracellular glutamine concentrations can lead to cell death known as glutamoptosis (Villar & Duran, 2017). It is compelling to speculate that parasites may use hGS both to benefit their own growth and to prevent induction of host death through the accumulation of the glutamine product until their development has been completed.

Schizonts in Z3 grow to larger sizes and would presumably be more likely successfully release larger numbers of infectious progenies into the circulation. It is unknown whether there are zonal differences in maturation, leading to successful release of the parasites into the circulation. Eickel and colleagues previously
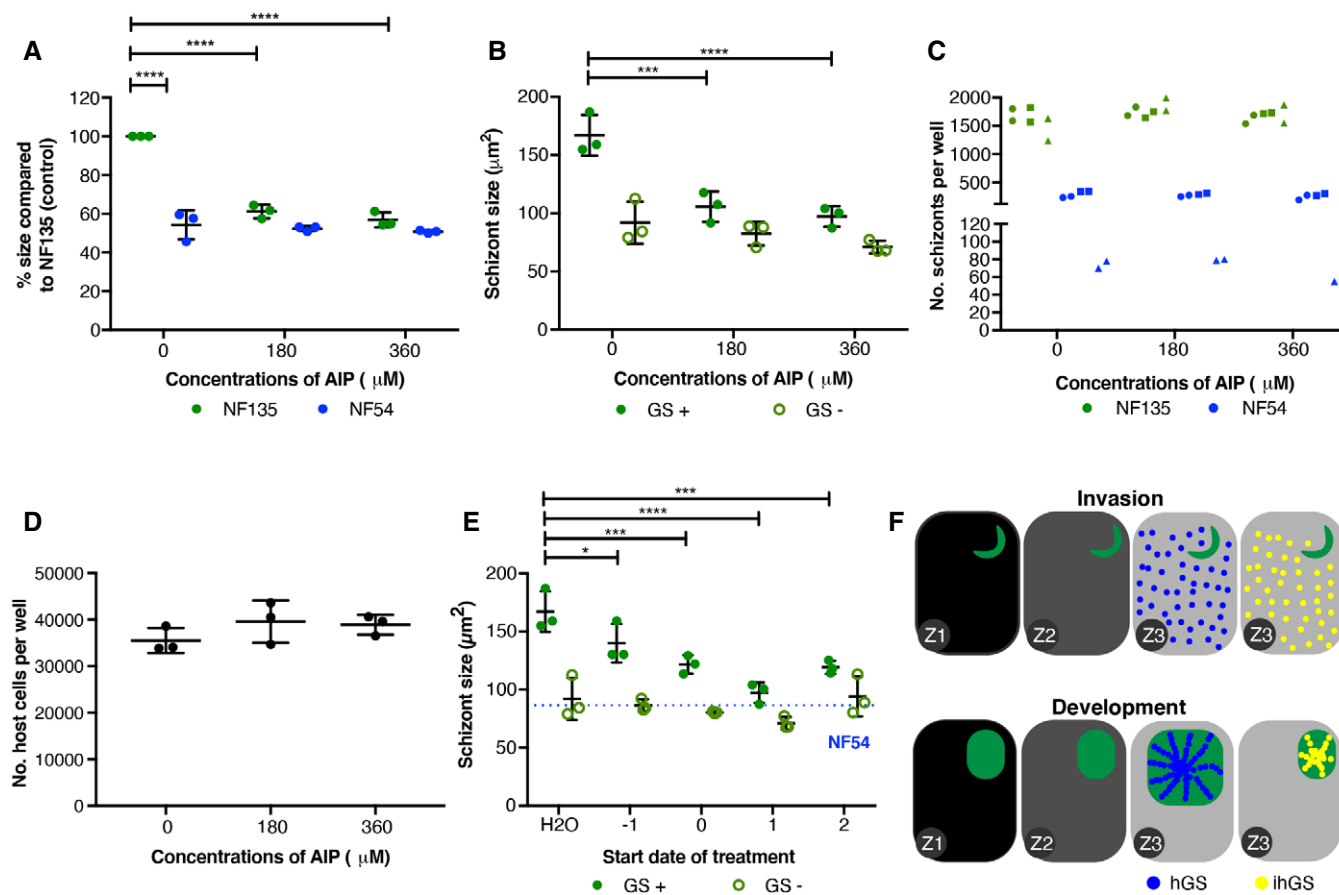
Figure 6. Effect of GS inhibitor on NF54 and NF135.

A Normalized percentage ±s.d. of intracellular schizont size of NF54 (blue) and NF135 (green) after treatment of GS inhibitors at different concentrations of AIP. Median size of the schizonts were normalized to that of H_2O-treated NF135 (which is set at 100%). AIP was added one day post-invasion and kept on for 48 h. Each dot represents a biological replicate where $\geq$ 100 schizonts were measured on day 5 p.i. A two-way ANOVA was performed followed by a Tukey's multiple comparison test with the ****$P < 0.0001$ to compare conditions within the same parasite strain. A two-way ANOVA was performed followed by a Sidak's multiple comparisons test with ****$P < 0.0001$ to compare conditions between parasite strains).

B Size difference between the GS-positive (closed circle) and GS-negative (open circle) NF135 schizonts after treatment of AIP. Each dot represents the median of a biological replicate where $\geq$ 100 schizonts were measured. Three biological replicates were performed with the median from each plotted ±s.d. A two-way ANOVA was performed followed by a Dunnett's multiple comparison test with ***$P = 0.0002$ and ****$P = 0.0001$.

C Number of schizonts per well for NF135 (green) and NF54 (blue). Three biological replicates (circle, square and triangle), each with two technical replicates were performed.

D Average ±s.d. (dot) host cell numbers per well for three independent biological replicates under the different AIP concentration.

E The difference in size between GS-positive (closed circle) and GS-negative (open circle) NF135 schizonts (day 5 p.i.) after treatment of AIP (360 μM) on different days pre- and post-invasion. Each dot represents the median size of $\geq$ 100 schizonts ±s.d. The dotted blue line shows the average median schizont size of NF54 treated with H_2O on day 5 post-invasion of the same three biological replicates. A two-way RM ANOVA was performed followed by a Tukey's multiple comparison test: *$P < 0.05$; **$P < 0.005$; ***$P < 0.001$; ****$P < 0.0001$.

F Summary of observed effects of hGS on parasite development. Sporozoites can invade Z1, 2 and 3 hepatocytes but disportionally prefer Z3 hepatocytes to make use of exclusive presence of hGS. Ability to uptake functional hGS early after invasion results in relatively larger schizonts; uptake of inhibited hGS (ihGS) reduces schizont size. (See Appendix Figs S3–S5 for raw measurements per replicate).

Source data are available online for this figure.

showed that the majority of the rodent malaria schizonts do not complete their maturation in hepatocytes (Eickel *et al*, 2013). Potential zonal differences in successful growth of liver stages and infection of red blood cells may have implications for therapeutic approaches: there is clear evidence that Z3 hepatocytes are involved in drug metabolism and transport (Tachikawa *et al*, 2018; Ahn *et al*, 2019). It would be intriguing to study whether infected Z3 can still maintain its drug metabolic function or whether pre-exposure to anti-malarial drugs has an effect on the growing schizonts and their progenies.

In summary, the combined data show that the developmental kinetics of *Pf* strains is most successful in a minority subset of hGS containing hepatocytes. Future identification of the complete set of host proteins present in hGS-positive Z3 hepatocytes will advance understanding of *Pf* interaction with host and may accelerate clinical development of novel intervention strategies against *Pf* liver stages.

Materials and Methods

Reagents and Tools table

Reagent/Resource	Reference or Source	Identifier or Catalog Number
Experimental models		
Human patient samples	Generated for this study	Ethics requires these samples to be anonymous
Recombinant DNA		
NA	NA	NA
Antibodies		
Rabbit PfHSP70 (1:75 dilution)	StressMarq Biosciences	SPC186
Mouse PfCSP (1:500 dilution)	MR4	2A10
Mouse PfEXP2 (1:1,000 dilution)	European Malaria Repository	7.7
Mouse PfGAPDH (1:50,000 dilution)	European Malaria Repository	7.2
Mouse PfMSP1 (1:100)	Sanaria and NIH/NIAD	AD233
Rabbit Human Glucokinase (1:100)	Abcam	ab88056
Mouse Human Glutamine Synthetase (1:100)	Abcam	ab64613
Alexa FluorTM 647 Phalloidin (1:45)	Thermofisher Scientific	A22287
Goat anti-rabbit Alexa Fluor 594 (1:200)	Thermofisher Scientific	A11012
Goat anti-mouse Alexa Fluor 488 (1:200)	Thermofisher Scientific	A11029
DAPI (300 nM)	Thermofisher Scientific	D1306
Oligonucleotides and sequence-based reagents		
PCR primers	This study (Sigma Aldrich)	Table EV1
Chemicals, enzymes and other reagents		
3-aminoimidazo[1,2-a]pyridine	Sigma Aldrich	685755
Glufosinate Ammonium	Sigma Aldrich	45520
L-Methionine sulfoximine	Sigma Aldrich	M5379
PierceTM 16% Formaldehyde, Methanol free (use at 4%)	Thermofisher Scientific	28906
Bovine Serum Albumin (use at 3%)	Sigma Aldrich	A9418
William's E medium with Glutamax	Thermofisher Scientific	32551-087
Insulin/Transferrin/Selenium	Thermofisher Scientific	41400-045
Sodium pyruvate	Thermofisher Scientific	11360-070
MEM-NEAA	Thermofisher Scientific	11140-035
Fungizone	Thermofisher Scientific	15290-018
Penicillin/streptomycin	Thermofisher Scientific	15140-122
Dexamethasone	Sigma Aldrich	D4902
Software		
FIJI—image analysis program	Schindelin *et al* (2012)	
Prism 7		
Other		
Leica DMI600B high content	Microscope	
Zeiss LSM880 with Airyscan	Microscope	

Methods and Protocols

Ethics statement

Primary human liver cells were freshly isolated from remnant surgical material. The samples are anonymized, and general approval for use of remnant surgical material was granted in accordance to the Dutch ethical legislation as described in the Medical Research (Human Subjects) Act and confirmed by the Committee on Research involving Human Subjects, in the region of Arnhem-Nijmegen, the Netherlands.

Characterization of genotype of parasite strains

Genomic DNA from different parasite strains were analysed for the presence/absence of GLURP; K1, MAD20, R033 allelic variant of MSP1; and the ICI and FC27 variant of MSP2 as described by McCall *et al* (2017). The primers used for genotyping can be found in Table EV1.

Generation of sporozoites for liver infection

Pf asexual and sexual blood stages were cultures in a semi-automatic system as described in (Ifediba & Vanderberg, 1981; Ponnudurai *et al*, 1982; Ponnudurai *et al*, 1989). *Anopheles stephensi* mosquitoes were reared in the Radboud University Medical Center insectary (Nijmegen, the Netherlands) according to standard operating procedures. Salivary glands from infected mosquitoes were hand dissected and collected in complete William's B medium [William's E medium with Glutamax (Thermo Fisher, 32551-087), supplemented with 1× insulin/transferrin/selenium (Thermo Fisher, 41400-045), 1 mM sodium pyruvate (Thermo Fisher, 11360-070), 1× MEM-NEAA (Thermo Fisher, 11140-035), 2.5 µg/ml Fungizone (Thermo Fisher 15290-018), 200 U/ml penicillin/streptomycin (Thermo Fisher 15140-122), and 1.6 µM dexamethasone (Sigma-Aldrich D4902-100MG)] without serum. After homogenization using home-made glass grinders, sporozoites were counted in a Burker-Turk chamber using phase contrast microscopy. Immediately before infection of human hepatocytes, the sporozoites are supplemented with heat inactivated human sera (HIHS) at 10% of total volume.

Primary human hepatocyte infection

Primary human hepatocytes were isolated from patients undergoing elective partial hepatectomy as described by Walk and colleagues (Walk *et al*, 2017). Freshly isolated hepatocytes suspended in complete Williams' B media were plated in 96 wells at 62,500 cells per well and kept in a 37°C (5% CO_2) incubator with daily media refreshments. Two days after plating, dissected sporozoites (day 16–21 post-blood meal) were added to the wells at 1:1 ratio in duplicates/triplicates and spun down at 1,811 *g* for 10 min on low brakes. Media was refreshed after 3 h to remove non-invaded sporozoites and then on a daily basis. The sporozoite-infected culture was maintained for 3 or 5 or 7 days after which the cells were fixed with 4% paraformaldehyde (Thermo Fisher Scientific: catalogue number 28906) for 10 min. The samples were permeabilized using 1% Triton and stained with the various *P. falciparum* or human antibodies listed in the Reagents Tools Table. The experiment(s) performed on the different liver segments are summarized in Table EV2.

GS inhibition

Three GS inhibitors were used to study the effect of GS on parasite infectivity and growth during liver stage development: 3-aminoimidazo[1,2-a]pyridine (Sigma-Aldrich; Cat no. 685755; AIP), Glufosinate-Ammonium (Sigma-Aldrich; Cat no. 45520; GA), and L-Methionine sulfoximine (Sigma-Aldrich; Cat no. M5379; LMS). They were tested in two concentrations: AIP (0.18 and 0.36 mM), GA (0.20 and 0.40 mM) and LMS (0.14 and 0.28 mM). Treatment period is for 48 h with one media refreshment in between after which the culture is returned to complete William's B media with 10% HIHS until day 5 post-invasion where the samples are fixed and stained for analysis by microscopy.

Microscopy

For this study, the Leica DMI6000B high content microscope was used for tiling 96 wells for determination of infection rate. For each well, a tile size of 9 × 9 was obtained at 20× objectives. The Zeiss LSM880 with Airyscan at 63× objectives (oil) and 2× zoom were used for detailed images.

Data analysis using FIJI

Infection rate

The tile consisting of 81 smaller images were merged in FIJI and saved as tiff files (Schindelin *et al*, 2012). Merged tiff files were opened in Adobe Photoshop and manually counted based on PfHSP70 positivity. For NF135 and NF175, only half the final tile (i.e. 40.5 images) were counted and then number of parasites were multiplied by two to get a final total number of parasites per well. Due to the lower infection rate of NF54, the whole tile is counted. Number of hepatic nuclei were counted for 1% of the total image and then multiplied by 100 to get final figure. Infection rate is calculated as total number of parasites (per well) divided by total number of host cells multiplied by 100.

Measurement of schizont size

Images obtained on the high content microscope were opened in FIJI. Random images were chosen until 100 parasites were measured (spread between two duplicate wells). Parasites were selected via the region of interest (ROI) tool using PfHSP70 positivity (red channel) and measured. In the cases, where the hGS intensity is required, the ROIs determined using PfHSP70 are masked onto the hGS channel (green) and then the measured. The RawIntDen values give the total signal measured in the ROI.

Quantifying intracellular hGS by immunofluorescence

For each of the image measured in the previous section, a total background intensity in the green channel (as hGS is labelled with Alexa-488) was determined using the region of interest (ROI). A background intensity per area (x) was determined (total intensity of whole image divided by area size of the image). A total background intensity for the parasite was determined by using the formula × multiplied by the measured size of the parasite. This is shown as the background (brown line) in Fig EV2A, B, D, E, G, H—the larger the parasite, the more total background in theory. Actual green intensity within a parasite is determined by using the ROI tool to just select the parasite in question (the "measured" line in Fig EV2A, B, D, E, G, H). The final "real" intensity of the parasite is calculated by subtracting the Background value from the Measured value and is what is plotted in Fig 5 and Appendix Fig S2.

Statistical analysis

For the majority of the experiments, three biological replicates were performed with either two or three technical replicates (depending on the availability of host cells and parasites). All statistical tests were performed using Prism 7. This includes calculating slope and correlation relationships. See figure legends and provided Excel sheet for details of statistical tests.

Data availability

This study includes no data deposited in external repositories.

Expanded View for this article is available online.

Author contributions

ASPY, YMW, G-JG, MV-B, and WG performed the experiments. JHWdW coordinated the collection of fresh human liver segments. ASPY and YMW collected the data and performed the analysis. ASPY, YMW, and RWS were involved in the conceptualization and writing of the manuscript.

Conflict of interest

The authors declare that they have no conflict of interest.

References

Ahn J, Ahn JH, Yoon S, Nam YS, Son MY, Oh JH (2019) Human three-dimensional *in vitro* model of hepatic zonation to predict zonal hepatotoxicity. *J Biol Eng* 13: 22

Aizarani N, Saviano A, Sagar ML, Durand S, Herman JS, Pessaux P, Baumert TF, Grun D (2019) A human liver cell atlas reveals heterogeneity and epithelial progenitors. *Nature* 572: 199−204

Ben-Moshe S, Shapira Y, Moor AE, Manco R, Veg T, Bahar Halpern K, Itzkovitz S (2019) Spatial sorting enables comprehensive characterization of liver zonation. *Nat Metab* 1: 899−911

Cory JG, Cory AH (2006) Critical roles of glutamine as nitrogen donors in purine and pyrimidine nucleotide synthesis: asparaginase treatment in childhood acute lymphoblastic leukemia. *In Vivo* 20: 587−589

Curi R, Lagranha CJ, Doi SQ, Sellitti DF, Procopio J, Pithon-Curi TC, Corless M, Newsholme P (2005) Molecular mechanisms of glutamine action. *J Cell Physiol* 204: 392−401

Eickel N, Kaiser G, Prado M, Burda PC, Roelli M, Stanway RR, Heussler VT (2013) Features of autophagic cell death in Plasmodium liver-stage parasites. *Autophagy* 9: 568−580

Fischer W, Ick M, Katz NR (1982) Reciprocal distribution of hexokinase and glucokinase in the periportal and perivenous zone of the rat liver acinus. *Hoppe Seylers Z Physiol Chem* 363: 375−380

Gill HS, Eisenberg D (2001) The crystal structure of phosphinothricin in the active site of glutamine synthetase illuminates the mechanism of enzymatic inhibition. *Biochemistry* 40: 1903−1912

Graumans W, Andolina C, Awandu SS, Grignard L, Lanke K, Bousema T (2019) *Plasmodium falciparum* gametocyte enrichment in peripheral blood samples by magnetic fractionation: gametocyte yields and possibilities to reuse columns. *Am J Trop Med Hyg* 100: 572−577

Guigas B, Bertrand L, Taleux N, Foretz M, Wiernsperger N, Vertommen D, Andreelli F, Viollet B, Hue L (2006) 5-Aminoimidazole-4-carboxamide-1-beta-D-ribofuranoside and metformin inhibit hepatic glucose phosphorylation by an AMP-activated protein kinase-independent effect on glucokinase translocation. *Diabetes* 55: 865−874

Gumucio JJ, Miller DL (1981) Functional implications of liver cell heterogeneity. *Gastroenterology* 80: 393−403

Halpern KB, Shenhav R, Matcovitch-Natan O, Toth B, Lemze D, Golan M, Massasa EE, Baydatch S, Landen S, Moor AE *et al* (2017) Single-cell spatial reconstruction reveals global division of labour in the mammalian liver. *Nature* 542: 352−356

Ifediba T, Vanderberg JP (1981) Complete *in vitro* maturation of *Plasmodium falciparum* gametocytes. *Nature* 294: 364−366

Jetton TL, Shiota M, Knobel SM, Piston DW, Cherrington AD, Magnuson MA (2001) Substrate-induced nuclear export and peripheral compartmentalization of hepatic glucokinase correlates with glycogen deposition. *Int J Exp Diabetes Res* 2: 173−186

Jungermann K (1983) Functional significance of hepatocyte heterogeneity for glycolysis and gluconeogenesis. *Pharmacol Biochem Behav* 18(Suppl 1): 409−414

Jungermann K, Kietzmann T (1996) Zonation of parenchymal and nonparenchymal metabolism in liver. *Annu Rev Nutr* 16: 179−203

Katz N, Teutsch HF, Jungermann K, Sasse D (1977) Heterogeneous reciprocal localization of fructose-1,6-bisphosphatase and of glucokinase in microdissected periportal and perivenous rat liver tissue. *FEBS Lett* 83: 272−276

Langenberg MCC, Wammes LJ, McCall MBB, Bijker EM, van Gemert GJ, Graumans W, van de Vegte-Bolmer MG, Teelen K, Hermsen CC, Koelewijn R *et al* (2018) Controlled human malaria infection with graded numbers of *Plasmodium falciparum* NF135.C10- or NF166.C8-infected mosquitoes. *Am J Trop Med Hyg* 99: 709−712

McCall MBB, Wammes LJ, Langenberg MCC, van Gemert GJ, Walk J, Hermsen CC, Graumans W, Koelewijn R, Franetich JF, Chishimba S *et al* (2017) Infectivity of *Plasmodium falciparum* sporozoites determines emerging parasitemia in infected volunteers. *Sci Transl Med* 9: eaag2490

Mo AX, McGugan G (2018) Understanding the liver-stage biology of malaria parasites: insights to enable and accelerate the development of a highly efficacious vaccine. *Am J Trop Med Hyg* 99: 827−832

Mowbray SL, Kathiravan MK, Pandey AA, Odell LR (2014) Inhibition of glutamine synthetase: a potential drug target in *Mycobacterium tuberculosis*. *Molecules* 19: 13161−13176

Odell LR, Nilsson MT, Gising J, Lagerlund O, Muthas D, Nordqvist A, Karlen A, Larhed M (2009) Functionalized 3-amino-imidazo[1,2-a]pyridines: a novel class of drug-like *Mycobacterium tuberculosis* glutamine synthetase inhibitors. *Bioorg Med Chem Lett* 19: 4790−4793

Ponnudurai T, Lensen AH, Leeuwenberg AD, Meuwissen JH (1982) Cultivation of fertile *Plasmodium falciparum* gametocytes in semi-automated systems. 1. Static cultures. *Trans R Soc Trop Med Hyg* 76: 812−818

Ponnudurai T, Lensen AH, Van Gemert GJ, Bensink MP, Bolmer M, Meuwissen JH (1989) Infectivity of cultured *Plasmodium falciparum* gametocytes to mosquitoes. *Parasitology* 98(Pt 2): 165−173

Rodrigues CD, Hannus M, Prudencio M, Martin C, Goncalves LA, Portugal S, Epiphanio S, Akinc A, Hadwiger P, Jahn-Hofmann K *et al* (2008) Host scavenger receptor SR-BI plays a dual role in the establishment of malaria parasite liver infection. *Cell Host Microbe* 4: 271−282

Ronzio RA, Rowe WB, Meister A (1969) Studies on the mechanism of inhibition of glutamine synthetase by methionine sulfoximine. *Biochemistry* 8: 1066−1075

Roth A, Maher SP, Conway AJ, Ubalee R, Chaumeau V, Andolina C, Kaba SA, Vantaux A, Bakowski MA, Thomson-Luque R *et al* (2018) A comprehensive model for assessment of liver stage therapies targeting *Plasmodium vivax* and *Plasmodium falciparum*. *Nat Commun* 9: 1837

Rowe WB, Ronzio RA, Meister A (1969) Inhibition of glutamine synthetase by methionine sulfoximine. Studies on methionine sulfoximine phosphate. *Biochemistry* 8: 2674−2680

Ruivo MTG, Vera IM, Sales-Dias J, Meireles P, Gural N, Bhatia SN, Mota MM, Mancio-Silva L (2016) Host AMPK is a modulator of plasmodium liver infection. *Cell Rep* 16: 2539−2545

Schindelin J, Arganda-Carreras I, Frise E, Kaynig V, Longair M, Pietzsch T, Preibisch S, Rueden C, Saalfeld S, Schmid B *et al* (2012) Fiji: an open-source platform for biological-image analysis. *Nat Methods* 9: 676−682

Seabra AR, Pereira PA, Becker JD, Carvalho HG (2012) Inhibition of glutamine synthetase by phosphinothricin leads to transcriptome reprograming in root nodules of *Medicago truncatula*. *Mol Plant Microbe Interact* 25: 976−992

Shears MJ, Sekhar Nirujogi R, Swearingen KE, Renuse S, Mishra S, Jaipal Reddy P, Moritz RL, Pandey A, Sinnis P (2019) Proteomic analysis of plasmodium merosomes: the link between liver and blood stages in malaria. *J Proteome Res* 18: 3404−3418

Silvie O, Rubinstein E, Franetich JF, Prenant M, Belnoue E, Renia L, Hannoun L, Eling W, Levy S, Boucheix C *et al* (2003) Hepatocyte CD81 is required for *Plasmodium falciparum* and *Plasmodium yoelii* sporozoite infectivity. *Nat Med* 9: 93−96

Sturm A, Amino R, van de Sand C, Regen T, Retzlaff S, Rennenberg A, Krueger A, Pollok JM, Menard R, Heussler VT (2006) Manipulation of host hepatocytes by the malaria parasite for delivery into liver sinusoids. *Science* 313: 1287−1290

Tachikawa M, Sumiyoshiya Y, Saigusa D, Sasaki K, Watanabe M, Uchida Y, Terasaki T (2018) Liver zonation index of drug transporter and metabolizing enzyme protein expressions in mouse liver acinus. *Drug Metab Dispos* 46: 610−618

Tarun AS, Peng X, Dumpit RF, Ogata Y, Silva-Rivera H, Camargo N, Daly TM, Bergman LW, Kappe SH (2008) A combined transcriptome and proteome survey of malaria parasite liver stages. *Proc Natl Acad Sci USA* 105: 305−310

Toyoda Y, Miwa I, Satake S, Anai M, Oka Y (1995) Nuclear location of the regulatory protein of glucokinase in rat liver and translocation of the regulator to the cytoplasm in response to high glucose. *Biochem Biophys Res Commun* 215: 467−473

Vera IM, Grilo Ruivo MT, Lemos Rocha LF, Marques S, Bhatia SN, Mota MM, Mancio-Silva L (2019) Targeting liver stage malaria with metformin. *JCI Insight* 4: e127441

Villar VH, Duran RV (2017) Glutamoptosis: a new cell death mechanism inhibited by autophagy during nutritional imbalance. *Autophagy* 13: 1078−1079

Walk J, Reuling IJ, Behet MC, Meerstein-Kessel L, Graumans W, van Gemert GJ, Siebelink-Stoter R, van de Vegte-Bolmer M, Janssen T, Teelen K *et al* (2017) Modest heterologous protection after *Plasmodium falciparum* sporozoite immunization: a double-blind randomized controlled clinical trial. *BMC Med* 15: 168

WHO (2018) World Malaria Report 2018.

Yalaoui S, Huby T, Franetich JF, Gego A, Rametti A, Moreau M, Collet X, Siau A, van Gemert GJ, Sauerwein RW *et al* (2008) Scavenger receptor BI boosts hepatocyte permissiveness to *Plasmodium* infection. *Cell Host Microbe* 4: 283−292